THE FUTURE OF PHOTOMETRIC, SPECTROPHOTOMETRIC AND POLARIMETRIC STANDARDIZATION
ASP Conference Series, Vol. 999, 2007
C. Sterken

Standard stars for linear polarization observed with FORS1

L. Fossati[1,2], S. Bagnulo[2], E. Mason[2], E. Landi Degl'Innocenti[3]

[1]*Institut fuer Astronomie, Universitaet Wien, Tuerkenschanzstrasse 17, A-1180 Wien, Austria*
[2]*European Southern Observatory, Alonso de Cordova 3107, Vitacura, Santiago, Chile*
[3]*Dipartimento di Astronomia e Scienza dello Spazio, Università di Firenze, Largo Enrico Fermi 2, I-50125 Firenze, Italy*

Abstract. We present the analysis of the observations of standard stars for linear polarization obtained from 1999 to 2005 within the context of the calibration plan of the FORS1 instrument of the ESO VLT. We have considered observations carried out both in imaging polarimetric and in spectropolarimetric mode. Broadband polarization was obtained in the Bessel *BVRI* filters; spectropolarimetry was obtained with various grisms covering different optical ranges and with a typical resolution of a few hundreds. Spectropolarimetric data have been convolved with the transmission functions of the Bessel filters, which enabled us to calculate polarization values equivalent to broadband polarization measurements in imaging mode. Finally, for each star, instrument mode, and for each Bessel filter band, we have calculated an average polarization value obtained after filtering all available data with a $k\sigma$-clipping algorithm.

1. Introduction

When taking polarimetric measurements of scientific targets, observations of standard stars for linear polarization are of crucial importance to calibrate and monitor instrument performances. Popular lists of standard stars are, e.g., those by Serkowski (1974) and Hsu and Breger (1998). Unfortunately, most of the 'classical' standard stars for polarization presented in these works are too bright for the instruments of the large size class telescopes.

At the ESO Very Large Telescope (VLT), observations of standard stars deemed to exhibit either zero polarization or substantial polarization are routinely performed within the context of the FORS1 calibration plan. Usually, a star known to exhibit a large signal of linear polarization is observed during those nights when a science target is observed in polarimetric mode. Occasionally, a non polarized star is also observed. However, the stability of these stars used as standard for linear polarization has never been extensively checked so far. Therefore, we have decided to retrieve from the archive a large sample of observations of polarimetric standard stars obtained with FORS1 and to check their consistency.

2. Instrument and observations

FORS1 is the visual and near ultraviolet **FO**cal **R**educer and low dispersion **S**pectrograph mounted at the Cassegrain focus of one of the four 8 m units of the ESO VLT, and works in the wavelength range $330 - 1100$ nm. FORS1 is equipped with polarization analyzing optics, which include a half-wave and a quarter-wave retarder plates, both superachromatic and a Wollaston prism with a beam divergence of 22”. This allows the measurement of linear and circular polarization, both in direct imaging and spectroscopy. In imaging polarimetric mode (IPOL) the field of view is $6.8' \times 6.8'$ and the magnitude limit is $R = 23$, for a 1 % accuracy in the polarization measure, and with 1 h exposure time. In spectropolarimetric mode (PMOS), the magnitude limit is between $R = 17.2$ and 19.3, for a spectral resolution between 260 and 1700 (with a 1” slit width, depending on the grism inserted). The instrument is described in Appenzeller et al. (1998).

We have retrieved from the ESO data archive (`http://archive.eso.org`) all observations of polarimetric standard stars taken with FORS1 from April 1999 to March 2005. A preliminary inspection to the data was performed to identify and discard a few saturated exposures and some frames with poor image quality. The list of the useful observations is presented in Table 1. About 210 observations in IPOL mode were obtained with the *BVRI* Bessel filters (observations with the *U* Bessel filter are not possible in polarimetric mode as the filter is situated in the same wheel as the Wollaston prism). About 130 observations in PMOS mode were obtained with a variety of grism and filter combinations. Both for IPOL and PMOS modes, the linear polarization was usually measured taking a series of four observations with the half wave retarder waveplate at $\alpha = 0°$, 22.5°, 45°, and 67.5°, respectively, where α indicates the angle between the acceptance axis of the ordinary beam of the Wollaston prism and the fast axis of the retarder waveplate. The acceptance axis of the Wollaston prism was always aligned to the North Celestial Meridian, which therefore represents the reference direction for all linear polarization measurements of this paper.

3. Data reduction

Stokes Q and U parameters are defined as in Landi Degl'Innocenti et al. (2007), with the reference axis coinciding with the North Celestial Meridian. In the following, we will consider the ratios Q/I and U/I, adopting the notation

$$P_Q = \frac{Q}{I} \text{ and } P_U = \frac{U}{I} . \tag{1}$$

P_Q and P_U were measured by combining the photon counts (background subtracted) of ordinary and extra-ordinary beams ($f^{\rm o}$ and $f^{\rm e}$, respectively) observed at retarder waveplate positions $\alpha = 0°$, 22.5°, 45°, and 67.5°, as given by the

Table 1. List of the observed stars. Sp. T. indicates the spectral type of the star. $N(\mathtt{I})$ and $N(\mathtt{P})$ indicate the numbers of observations in IPOL and PMOS mode respectively. Type indicates if the star is a candidate polarized standard star (P) or unpolarized standard star (nP)

RA J2000	DEC J2000	Id 1	Id 2	V	Sp. T.	$N(\mathtt{I})$	$N(\mathtt{P})$	Type
05:36:23.01	21:11:11.4	HD 245310	BD+21 901	8.96	B2e	0	2	P
05:41:37.85	−01:54:36.5	NGC 2024 1	JP11 3950	12.17	B0	15	12	P
06:05:05.67	23:23:38.5	HD 251204	BD+23 453	10.20	B0	0	1	P
06:06:41.04	−42:17:55.7	HD 42078	CD−42 2343	6.16	Am	0	6	P
09:06:00.01	−47:18:58.2	Ve 6−23	GSC 08169−00417	12.12	B0V	45	23	P
12:51:03.56	−61:14:37.7	HD 111579	CD−60 4390	9.17	B2	0	3	P
14:28:50.87	−60:32:25.1	HD 126593	CD−59 5269	8.67	B1	0	1	P
16:18:43.73	−51:27:57.8	CD −51 9993	TYC 8323−1798−1	10.25	B	3	0	P
17:12:19.95	−04:24:09.3	HD 155528	BD−04 4244	9.62	B9	1	2	P
17:43:19.59	−28:40:32.8	CD −28 13479	Hilt 652	10.80	B1	26	16	P
17:43:47.02	−07:04:46.6	HD 161056	BD−07 4487	630	B1	2	2	P
17:45:43.70	−29:13:18.1	HD 316232	CD−29 13940	10.40	O	9	6	P
18:11:58.10	−14:56:09.0	BD −14 4922	Hilt 715	9.73	O9	11	7	P
18:40:01.70	−12:24:06.9	BD −12 5133	Hilt 781	10.40	B1V	31	9	P
18:41:22.57	−13:50:28.9	BD −13 5073	Hilt 785	10.40	B1e	4	2	P
00:02:10.75	−43:09:55.6	WD 2359−434	GJ 915	13.05	DAs	9	0	nP
01:37:18.59	−40:10:38.5	HD 10038	CD−40 404	8.14	A2m	1	4	nP
01:57:56.14	−02:05:57.7	HD 12021	BD−02 329	8.85	A0	0	1	nP
02:11:16.69	−46:35:06.2	HD 13588	CD−47 663	7.90	A1m	1	5	nP
02:35:07.60	03:43:56.8	WD 0232+035	Feige 24	12.40	DAw	0	1	nP
03:10:31.02	−68:36:03.4	WD 0310−688	TYC 9145−601−1	11.10	DA	6	0	nP
07:52:25.51	−23:17:46.8	HD 64299	BD−22 2058	10.11	A1V	0	2	nP
07:53:08.38	−67:47:32.2	WD 0752−676	GJ 293	14.09	DC	9	0	nP
11:13:50.74	−52:51:21.2	HD 97689	CD−52 4222	6.82	A0m	0	3	nP
16:17:55.25	−15:35:52.4	WD 1615−154	G 153−41	12.40	DA	6	6	nP
16:23:33.84	−39:13:46.2	WD 1620−391	CD−38 10980	11.00	DA	16	3	nP
19:02:08.52	−41:54:37.8	HD 176425	CD−42 13839	6.21	A0V	1	2	nP
20:10:56.85	−30:13:06.6	WD 2007−303	CD−30 17706	12.18	DA	0	5	nP
20:42:34.75	−20:04:35.9	WD 2039−202	HIP 102207	12.34	DAw	5	5	nP
21:52:25.38	02:23:19.6	WD 2149+021	HIP 107968	12.73	DA	7	3	nP

following formula:

$$
\begin{aligned}
P_Q &= \frac{1}{2}\left\{ \left(\frac{f^{\rm o}-f^{\rm e}}{f^{\rm o}+f^{\rm e}}\right)_{\alpha=0^\circ} - \left(\frac{f^{\rm o}-f^{\rm e}}{f^{\rm o}+f^{\rm e}}\right)_{\alpha=45^\circ} \right\} \\
P_U &= \frac{1}{2}\left\{ \left(\frac{f^{\rm o}-f^{\rm e}}{f^{\rm o}+f^{\rm e}}\right)_{\alpha=22.5^\circ} - \left(\frac{f^{\rm o}-f^{\rm e}}{f^{\rm o}+f^{\rm e}}\right)_{\alpha=67.5^\circ} \right\}
\end{aligned}
\tag{2}
$$

(see FORS1/2 User manual, VLT-MAN-ESO-13100-1543). The error on P_Q or P_U is

$$
\begin{aligned}
\sigma^2_{P_X} = & \left(\left(\frac{f^{\rm e}}{(f^{\rm o}+f^{\rm e})^2}\right)^2 \sigma^2_{f^{\rm o}} + \left(\frac{f^{\rm o}}{(f^{\rm o}+f^{\rm e})^2}\right)^2 \sigma^2_{f^{\rm e}} \right)_{\alpha=\phi_0} + \\
& \left(\left(\frac{f^{\rm e}}{(f^{\rm o}+f^{\rm e})^2}\right)^2 \sigma^2_{f^{\rm o}} + \left(\frac{f^{\rm o}}{(f^{\rm o}+f^{\rm e})^2}\right)^2 \sigma^2_{f^{\rm e}} \right)_{\alpha=45^\circ+\phi_0} ,
\end{aligned}
\tag{3}
$$

where $\phi_0 = 0^\circ$ if $X = Q$ and $\phi_0 = 22.5^\circ$ if $X = U$. If the polarization of the targets is always small, in order to give an estimate of the quantities σ_{P_X} one can substitute in Eq. (3) $f^{\rm e} = f^{\rm o} = f$, with f independent of α. Also, if one can assume $\sigma_{f^{\rm e}} = \sigma_{f^{\rm o}} = \sigma_f$ we have

$$\sigma_{P_X} = \frac{\sigma_f}{f} \; . \tag{4}$$

If the error on the photon counts is entirely due to photon-counts, we get

$$\sigma_{P_X} = \frac{1}{2}\,\frac{1}{\sqrt{f}} \; . \tag{5}$$

From P_Q and P_U we have obtained the total fraction of linear polarization $P_{\rm L}$ and the position angle θ (see Landi Degl'Innocenti et al. 2007). For the cases where polarimetric errors are small with respect to the signal ($\sigma_{P_{\rm Q}} \ll P_{\rm L}$, $\sigma_{P_{\rm U}} \ll P_{\rm L}$), the errors on $P_{\rm L}$ and θ are

$$\sigma_{P_{\rm L}} = \left[\cos^2(2\theta)\sigma^2_{P_Q} + \sin^2(2\theta)\sigma^2_{P_U}\right]^{1/2} \tag{6}$$

$$\sigma_\theta = \frac{1}{2}\frac{\left[\sin^2(2\theta)\sigma^2_{P_Q} + \cos^2(2\theta)\sigma^2_{P_U}\right]^{1/2}}{P_{\rm L}} \; . \tag{7}$$

Note that if $\sigma_{P_Q} = \sigma_{P_U}$ one gets

$$\sigma_{P_{\rm L}} = \sigma_{P_Q} = \sigma_{P_U} \tag{8}$$

and

$$\sigma_\theta = \frac{1}{2}\,\frac{\sigma_{P_L}}{P_{\rm L}} \; . \tag{9}$$

3.1. IPOL data

All the science frames were bias subtracted using the corresponding master bias obtained from a series of five frames taken the morning after the observations. No flat-field correction was carried out as it is irrelevant for the purpose of measuring the polarization through Eq. (2). The flux in the ordinary and extra-ordinary beams was measured via simple aperture photometry, that was performed using the `DAOPHOT` package implemented in `IRAF`. Once the fluxes for the ordinary and extraordinary beams for each retarder waveplate position were measured, we used a dedicated C routine to calculate P'_Q and P'_U through Eq. (2), the corresponding errors via Eq. (3), then the fraction of linear polarization $P'_{\rm L}$ and the position angle θ' with Eqs. (6) and (7) of Landi Degl'Innocenti et al. (2007), with the corresponding errors given in Eqs. (6) and (7) of this paper. To compensate a chromatism problem of the half wave plate (see Sect. 3.2) a new position angle θ was obtained as

$$\theta = \theta' - \epsilon_\theta({\rm F}) \tag{10}$$

where $\epsilon_\theta({\rm F})$ is a correction factor that depends upon the filter F. The $\epsilon_\theta({\rm F})$ values are tabulated in the FORS1/2 user manual (see also `http://www.eso.org/instruments/fors/inst/pola.html`). We obtained the final P_Q and P_U values as

$$\begin{array}{rcl} P_Q &=& P'_{\rm L}\,\cos(2\theta) \\ P_U &=& P'_{\rm L}\,\sin(2\theta)\,. \end{array} \tag{11}$$

with θ given by Eq. (10) (note that $P_{\rm L} = P'_{\rm L}$).

3.2. PMOS data

PMOS data were pre-processed with the packages for spectra analysis implemented in IRAF. Spectra in the ordinary and extraordinary beams were bias-subtracted, then optimally extracted and wavelength calibrated using IRAF routines, and finally processed using dedicated C routines to calculate P_Q, P_U, $P_{\rm L}$, and θ with the corresponding errors using Eqs. (2) and (3) of this paper, and Eqs. (6) and (7) of Landi Degl'Innocenti et al. (2007).

Figure 1 shows the results for the star Ve 6-23 observed in the night 17 December 2003 with the 150 I grism and the GG 435 filter. The position angle of interstellar polarization is expected to have a constant value independent of wavelength. The botton right panel of Fig. 1 shows that this is not the case for the star Ve 6-23 (as well as for all other stars of our sample). This is due to a chromatism problem of the half-wave retarder waveplate already discussed in Sect. 3.1.

To compare the IPOL with the PMOS observations we convolved the polarized spectra obtained in PMOS with the transmission functions of the *BVRI* Bessel filters used in IPOL mode. For each filter F we calculated

$$P_Q({\rm F}) = \frac{\int_0^\infty {\rm d}\lambda\, P_Q(\lambda) I_Q(\lambda) T_{\rm F}(\lambda)}{\int_0^\infty {\rm d}\lambda\, I_Q(\lambda) T_{\rm F}(\lambda)} \qquad P_U({\rm F}) = \frac{\int_0^\infty {\rm d}\lambda\, P_U(\lambda) I_U(\lambda) T_{\rm F}(\lambda)}{\int_0^\infty {\rm d}\lambda\, I_U(\lambda) T_{\rm F}(\lambda)} \tag{12}$$

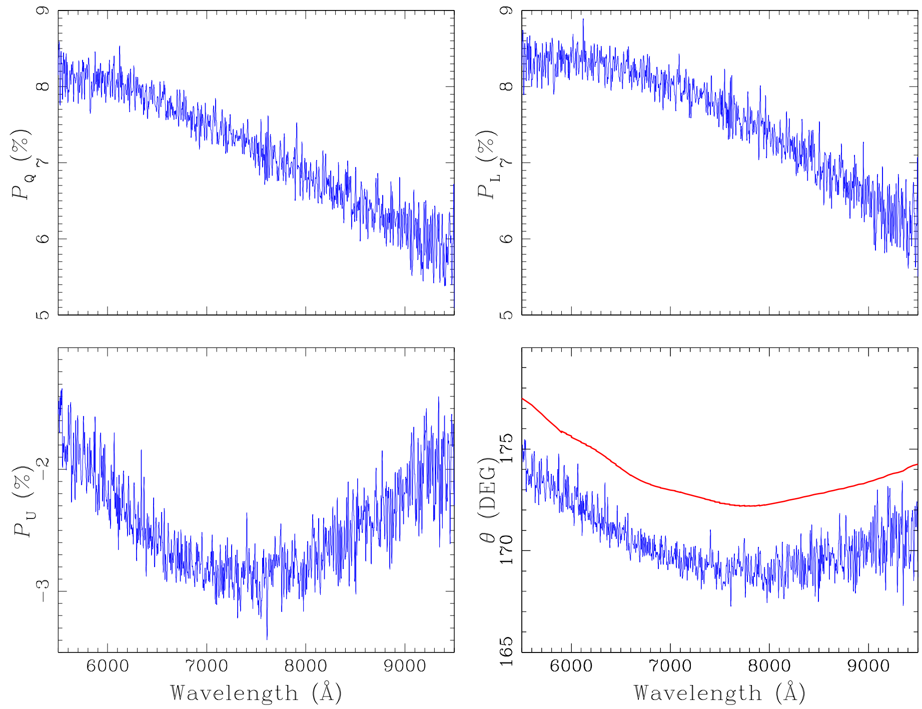

Figure 1. Star Ve 6-23: P'_Q, P'_U, $P_{\rm L}$, and θ' observed in the night 17 December 2003 with grism 150 I and filter GG435. The non-constant θ value is due to the chromatism of the half waveplate. The thin solid line shows the offset angle $\epsilon_\theta(\lambda)$ (data are available at `http://www.eso.org/instruments/fors/inst/pola.html`) that has to be subtracted to the observed position angle to compensate for the waveplate chromatism (in the figure, $\epsilon_\theta(\lambda)$ is offset by a constant to allows its visualization).

where $T_{\rm F}$ is the transmission function of the F filter, and

$$\begin{array}{rcl} I_Q & = & (f^{\rm o} + f^{\rm e})\,|_{\alpha=0^\circ} + (f^{\rm o} + f^{\rm e})\,|_{\alpha=45^\circ} \\ I_U & = & (f^{\rm o} + f^{\rm e})\,|_{\alpha=22.5^\circ} + (f^{\rm o} + f^{\rm e})\,|_{\alpha=67.5^\circ}\ . \end{array} \tag{13}$$

The polarization values so obtained have been finally modified according to the procedure followed for the IPOL data, in order to compensate for the chromatism of the half wave plate.

Error bars obtained in PMOS mode are smaller than those obtained in IPOL mode. This is a consequence of the fact that the signal-to-noise ratio of the observations is basically limited by the full well capacity of the CCD pixels, or by the hardware limitations of the digital-analogic converter. Rebinning spectropolarimetric data permits one to integrate the signal over a much higher number of pixels than possible in imaging mode, leading to a much higher signal-to-noise ratio. A comparison between IPOL and rebinned PMOS data can be seen in Figs. 2 and 3 for stars Ve 6-23 and CD −28 13479, respectively, in the B band.

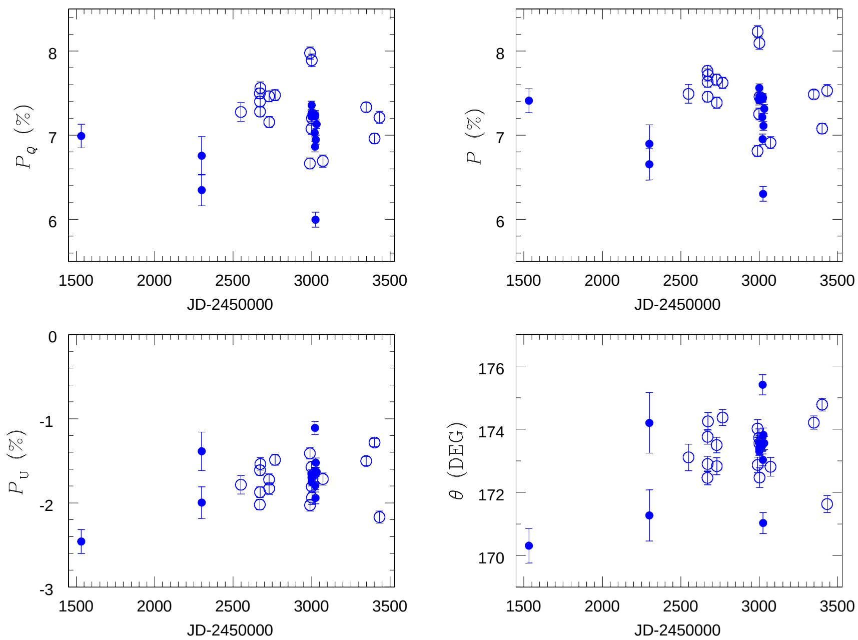

Figure 2. IPOL data (full circles) and rebinned PMOS data (open circles) for the star Ve 6-23 in the B band

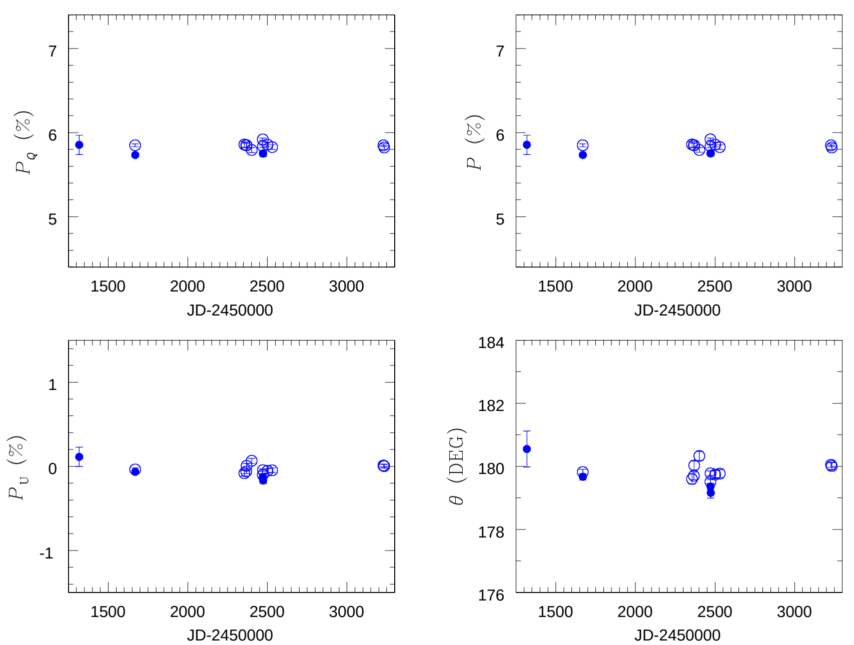

Figure 3. IPOL data (full circles) and rebinned PMOS data (open circles) for the star CD -28 13479 in the B band

4. Results and discussion

Figures 2 and 3 show the polarization observed in IPOL and in PMOS mode for stars Ve 6-23 and CD −28 13479, respectively, plotted as a function of the observation epoch. The plot scales are the same for both stars. The data for the star Ve 6-23 appear much more scattered than those for the star CD −28 13479. Whereas some scattering may well be due to undetected instrument or data reduction problems, Fig. 2 suggests that the polarization of the star Ve 6-23 may exhibit a short-term variability.

For each star, we have grouped all observations obtained with similar instrument mode and with the same filter (or convolved with the same trasmission function, in case of PMOS observations). From each group so obtained we have calculated the medians of the observed P_Q and P_U values, $\widetilde{P_X}$ (with $X = Q$ and U), and the median absolute deviations (MAD), i.e., the medians of the distributions

$$|(P_X)_i - \widetilde{P_X}| \, . \tag{14}$$

Setting $\sigma = 1.48\,\mathrm{MAD}$ (e.g., Huber 1981, pp. 107–108), we have then rejected those $(P_X)_i$ values for which

$$|(P_X)_i - \widetilde{P_X}| > 3\,\sigma \tag{15}$$

Finally, from the remaining values, we have calculated the weighted averages $\widehat{P_Q}$ and $\widehat{P_U}$:

$$\widehat{P_X} = \frac{\sum_i \frac{(P_X)_i}{(\sigma^2_X)_i}}{\sum_i \frac{1}{(\sigma^2_X)_i}} \, . \tag{16}$$

To each average value, we have associated the error given by

$$\sigma^2_{P_X} = \frac{1}{N-1} \, \frac{\sum_i \frac{\left((P_X)_i - \widehat{P_X}\right)^2}{(\sigma^2_{P_X})_i}}{\sum_i \frac{1}{(\sigma^2_{P_X})_i}} \tag{17}$$

The results are shown in Table 2 (for the stars with high polarization signal) and 3 (for the stars with low polarization signal). Stars observed only once were not included in the tables. For stars with less than four observations we did not run the $k\sigma$-clipping algorithm.

4.1. Polarized stars

Table 2 may be used as a reference to check instrument performance and stability within the quoted error bars, both in IPOL and PMOS mode. Note that relatively large errors may point to a star's instrisic variability, especially if large errors are associated to large data sets. Observations within similar filter bands are fairly, but not always fully consistent, see Sect. 4.2 below.

It should be noted that the actual correction that has to be applied to the broadband polarization measurements to compensate for the chromatism of the retarder waveplate depends on the shape of the star's spectral energy distribution (convolved with the transmission of the telescope optics). In fact, we have applied a correction that is independent of the star's colour. This is probably the reason why the position angles of the stars of Table 2 are slightly filter dependent. For the same reason, caution should be adopted when comparing the results reported in Table 2 with polarimetric observations obtained with other instruments.

4.2. Unpolarized stars

All stars observed in IPOL mode and reported in Table 3 have P_Q and P_U values consistent with zero. This means that all these stars may be considered as unpolarized standard stars within a typical accuracy better than 3×10^{-4}. At the same time, the available IPOL observations do not show evidence for significant instrumental polarization *in the center of the instrument field of view*[1].

WD 2007-303, that was observed in PMOS mode only, is polarized at about 0.5 % level in P_Q, and should not be used as unpolarized standard star.

The remaining PMOS observations hint that there is a small instrumental offset in P_Q. The weigthed average of all P_Q values of Table 3 (but without considering the star WD 2007-303) is $P_Q(B)|_0 = 0.07 \pm 0.01\,\%$, and $P_Q(V)|_0 = 0.09 \pm 0.01\,\%$ for the B and the V filter, respectively (the errors were calculated with Eq. (17)). The averages of all P_U values of Table 3 is fully consistent with 0 (with an error bar of about 0.005 %) both in the B and in the V filters. The observed P_Q offset, that appears instrinsic to the PMOS mode only, may be associated to some but not all grism+filter combinations, and deserves further investigation.

Acknowledgments. L. Fossati acknowledges ESO DGDF for a four month studentship at ESO Santiago/Vitacura.

References

Appenzeller, I., Fricke, K., Furtig, W., et al., 1998, The Messenger, 94, 1
Huber, P. J. 1981, Robust Statistics, J. Wiley & Sons, New York
Hsu, J.-C., & Breger, M., 1982, ApJ, 262
Landi Degl'Innocenti, E., Bagnulo, S., & Fossati, L., 2007, these Proceedings
Patat, F., & Romaniello, M., 2006, PASP, 118, 146
Serkowski, K., 1974, in: Planets, stars and nebulae studied with photopolarimetry, T. Gehrles (ed.) University of Arizona press, p. 135

[1]For a study of the FORS1 instrumental polarization off-axis see Patat & Romaniello (2006)

Table 2.: Weighted averages of the observations of polarized stars in IPOL and PMOS mode with various instrument settings. The averages were calculated after running the $k\sigma$-clipping procedure explained in the text. N_s and N_e represent the number of data before and after running the $k\sigma$-clipping procedure, respectively. Note that for $N \leq 3$ no $k\sigma$-clipping procedure was applied.

Star	Mode	Filter	P_Q (%)	P_U (%)	P (%)	θ	N_s	N_e
HD 245310	PMOS	V	−1.02±0.02	−3.98±0.01	4.10±0.01	127.79±0.12	2	2
NGC 2024 1	IPOL	B	0.80±0.07	−8.28±0.01	8.31±0.01	137.77±0.24	6	4
	IPOL	V	0.16±0.20	−9.64±0.06	9.65±0.06	135.47±0.59	3	3
	IPOL	R	0.28±0.01	−9.62±0.01	9.62±0.01	135.84±0.02	4	3
	IPOL	I	0.40±0.05	−9.11±0.04	9.12±0.04	136.26±0.15	2	2
	PMOS	B	1.05±0.09	−8.02±0.06	8.09±0.06	138.75±0.32	10	9
	PMOS	V	0.58±0.05	−9.51±0.02	9.53±0.02	136.74±0.16	10	9
Ve 6-23	IPOL	B	7.12±0.05	−1.66±0.02	7.32±0.05	173.42±0.10	14	11
	IPOL	V	7.91±0.05	−2.38±0.06	8.26±0.05	171.61±0.21	12	10
	IPOL	R	7.56±0.06	−2.32±0.03	7.90±0.05	171.47±0.13	13	12
	IPOL	I	6.88±0.06	−2.28±0.08	7.25±0.07	170.86±0.31	5	4
	PMOS	B	7.24±0.08	−1.68±0.06	7.43±0.08	173.48±0.23	17	17
	PMOS	V	7.98±0.02	−2.29±0.04	8.30±0.02	171.99±0.12	13	13
	PMOS	R	7.76±0.01	−2.24±0.01	8.08±0.01	171.97±0.03	2	2
	PMOS	I	7.02±0.06	−2.01±0.02	7.31±0.06	172.02±0.11	6	5
HD 111579	PMOS	B	−5.21±0.18	−2.23±0.56	5.67±0.29	101.60±2.56	2	2
	PMOS	V	−5.73±0.03	−2.49±0.21	6.25±0.10	101.76±0.87	2	2
CD-28 13479	IPOL	B	5.70±0.01	−0.11±0.03	5.70±0.01	179.47±0.13	4	3
	IPOL	V	6.24±0.03	−0.18±0.04	6.25±0.03	179.18±0.20	6	6
	IPOL	R	6.07±0.02	−0.13±0.02	6.07±0.02	179.39±0.10	15	11
	PMOS	B	5.80±0.01	−0.03±0.01	5.80±0.01	179.85±0.05	11	9
	PMOS	V	6.31±0.01	−0.16±0.02	6.32±0.01	179.27±0.07	14	13
	PMOS	I	5.61±0.04	−0.16±0.02	5.61±0.04	179.18±0.11	2	2
HD 316232	IPOL	V	4.85±0.02	0.41±0.07	4.87±0.02	2.40±0.38	3	3
	IPOL	R	4.69±0.03	0.55±0.02	4.72±0.03	3.36±0.12	3	3
	IPOL	I	4.32±0.01	0.40±0.04	4.34±0.01	2.65±0.26	2	2
	PMOS	B	4.62±0.02	0.57±0.01	4.66±0.02	3.54±0.06	4	4
	PMOS	V	4.97±0.01	0.51±0.02	5.00±0.01	2.94±0.10	3	3
BD-14 4922	IPOL	B	−0.98±0.03	5.63±0.01	5.71±0.01	49.93±0.15	4	4
	IPOL	V	−0.99±0.02	6.07±0.02	6.15±0.02	49.62±0.08	5	5
	IPOL	R	−0.98±0.05	5.69±0.07	5.77±0.07	49.90±0.24	2	2
	PMOS	B	−0.97±0.01	5.66±0.01	5.74±0.01	49.88±0.07	5	4
	PMOS	V	−0.93±0.01	6.06±0.01	6.13±0.01	49.35±0.03	5	3
	PMOS	I	−0.70±0.03	5.07±0.01	5.12±0.01	48.92±0.19	2	2
BD-12 5133	IPOL	B	1.87±0.04	−3.95±0.05	4.37±0.05	147.64±0.28	6	5
	IPOL	V	1.75±0.04	−4.00±0.04	4.37±0.04	146.84±0.25	5	4
	IPOL	R	1.63±0.02	−3.68±0.02	4.02±0.02	146.97±0.13	16	13
	IPOL	I	1.10±0.29	−3.39±0.07	3.57±0.09	143.99±2.27	3	3
	PMOS	B	1.94±0.04	−3.94±0.03	4.39±0.03	148.09±0.23	5	4
	PMOS	V	1.80±0.04	−4.05±0.01	4.43±0.02	146.99±0.22	6	4
	PMOS	I	1.03±0.47	−3.37±0.06	3.53±0.11	143.45±3.73	2	2
BD-13 5073	IPOL	R	2.10±0.01	−2.99±0.03	3.66±0.02	152.55±0.11	2	2
	PMOS	V	3.40±1.59	−2.64±1.17	4.30±1.47	161.11±8.77	2	2

Table 3.: Weighted averages of the observations of unpolarized stars in IPOL and PMOS mode with various instrument settings. The meaning of the various columns is the same as in Table 2

Star	Mode	Filter	P_Q (%)	P_U (%)	N_s	N_e
WD 2359-434	IPOL	R	0.03±0.06	−0.20±0.09	4	4
	IPOL	I	−0.00±0.01	0.03±0.04	4	4
HD 10038	PMOS	B	0.07±0.01	−0.03±0.02	3	3
	PMOS	V	0.11±0.01	−0.03±0.01	2	2
HD 13588	PMOS	B	0.10±0.01	0.00±0.01	4	4
	PMOS	V	0.10±0.01	0.00±0.01	4	4
WD 0310-688	IPOL	V	0.01±0.04	−0.05±0.10	3	3
	IPOL	R	0.04±0.09	0.01±0.14	2	2
HD 42078	PMOS	B	0.04±0.01	−0.01±0.01	4	2
	PMOS	V	0.07±0.01	−0.02±0.01	6	6
HD 64299	PMOS	B	−0.02±0.12	−0.04±0.04	2	2
	PMOS	V	−0.05±0.13	−0.03±0.04	2	2
WD 0752-676	IPOL	B	−0.00±0.01	0.06±0.03	4	3
	IPOL	V	0.00±0.01	0.03±0.05	3	3
HD 97689	PMOS	B	0.16±0.04	0.01±0.01	3	3
	PMOS	V	0.14±0.08	−0.00±0.01	2	2
WD 1615-154	IPOL	V	0.03±0.24	−0.05±0.03	2	2
	IPOL	R	−0.01±0.04	−0.02±0.12	2	2
	PMOS	B	0.07±0.02	−0.03±0.02	5	5
	PMOS	V	0.13±0.01	−0.02±0.02	4	4
WD 1620-391	IPOL	B	0.02±0.03	−0.02±0.02	3	3
	IPOL	V	−0.01±0.01	−0.01±0.01	4	3
	IPOL	R	−0.00±0.01	0.01±0.01	5	4
	IPOL	I	0.01±0.01	0.01±0.01	4	2
	PMOS	B	0.06±0.02	0.00±0.01	2	2
	PMOS	V	0.08±0.02	0.00±0.01	2	2
HD 176425	PMOS	V	0.15±0.13	−0.08±0.06	2	2
WD 2007-303	PMOS	B	0.44±0.01	−0.09±0.01	4	3
	PMOS	V	0.51±0.02	−0.05±0.01	4	4
WD 2039-202	IPOL	R	0.19±0.23	−0.14±0.40	2	2
	PMOS	B	0.03±0.03	0.00±0.01	2	2
	PMOS	V	0.03±0.01	−0.00±0.01	2	2
	PMOS	I	0.10±0.01	0.01±0.01	2	2
WD 2149+021	IPOL	V	0.01±0.03	−0.04±0.01	2	2
	IPOL	R	0.14±0.14	−0.02±0.09	3	3
	PMOS	V	0.09±0.01	−0.01±0.03	2	2
	PMOS	I	0.16±0.01	−0.01±0.04	2	2